remote sensing

MDPI

Article

Detection Ground Deformation Characteristics of Reclamation Land with Time-Series Interferometric Synthetic Aperture Radar in Tianjin Binhai New Area, China

Yanan Chen [1,2], Fuli Yan [2,*], Jian Chen [1] and Xiangtao Fan [2]

[1] College of Engineering and Technology, China University of Geosciences-Beijing, 029 Xueyuan Road, Beijing 100083, China; 3002210024@email.cugb.edu.cn (Y.C.); jianchen@cugb.edu.cn (J.C.)
[2] Aerospace Information Research Institute, University of Chinese Academy of Sciences, 009 Deng Zhuang South Road, Beijing 100094, China; fanxt@radi.ac.cn
* Correspondence: yanfl@radi.ac.cn; Tel.: +86-136-9159-7215

Abstract: In order to alleviate the conflict between populations and land resource, Tianjin adopted multi-phase reclamation projects to the formed large-scale artificial reclamation land. The reclamation areas, however, are prone to subsidence, which poses a significant threat to infrastructure as well as the safety and assets of the residents. The SBAS-InSAR was used to acquire surface deformation of Tianjin Binhai New Area from January 2017 to December 2022, analyze in depth the response relationship between land subsidence, reclamation project time, and land-use type. There is a strong correlation between surface deformation and reclamation time. Severe land subsidence occurred over newly reclaimed areas. In the offshore direction, the deformation values of the Nangang Industrial Zone, the Lingang Industrial Zone, and Hangu Harbor were −98 mm to −890 mm, 45 mm to −580 mm, and −140 mm to −290 mm, respectively. Significant differences in deformation were detected among different land-use types where reclamation projects were completed in the same time. Subsidence was positively correlated with surface load; in areas with higher surface loads, the surface settlement was also more severe. The average surface settlement for the heavy shipyard, with 67 grain storage tanks and 27 grain storage tanks, road, and bare land were −201 mm, −166 mm, −107 mm, −64 mm, and −43 mm, respectively. This study reveals significant differences of surface deformation in the reclamation completed at different times, and determines that the load is the main driving factor of settlement difference in the reclamation land completed at the same time. This has important guiding significance for preventing and controlling geological disasters in the reclamation area and later development planning.

Keywords: ground settlement; marine reclamation land; SBAS-InSAR; Tianjin Binhai new area

check for updates

Citation: Chen, Y.; Yan, F.; Chen, J.; Fan, X. Detection Ground Deformation Characteristics of Reclamation Land with Time-Series Interferometric Synthetic Aperture Radar in Tianjin Binhai New Area, China. *Remote Sens.* **2023**, *15*, 5303. https://doi.org/10.3390/rs15225303

Academic Editors: Mimmo Palano, Giuseppe Pezzo, Michele Mangiameli, Giuseppe Mussumeci and Stefano Gandolfi

Received: 2 September 2023
Revised: 26 October 2023
Accepted: 31 October 2023
Published: 9 November 2023

Copyright: © 2023 by the authors. Licensee MDPI, Basel, Switzerland. This article is an open access article distributed under the terms and conditions of the Creative Commons Attribution (CC BY) license (https://creativecommons.org/licenses/by/4.0/).

1. Introduction

With the rapid development of urbanization, the demand for land resources is increasing sharply. Land reclamation has become an important method of alleviating population density pressure. China [1,2], USA [3], Singapore [4], Ireland [5], and other countries [6] have carried out large-scale land reclamation projects. Both dredger fill layer and underlying soil layer undergo consolidation compaction, and the compaction of the sedimentary strata is considered to be an important factor causing land subsidence in the reclamation land [7]. Therefore, the land subsidence of artificial reclamation areas worldwide is inevitable. Tianjin is a modern coastal metropolis with a permanent population of 15.6 million as of 2008 and an urbanization rate as high as 83.15% [8]. Tianjin Binhai New Area has expanded its urban space through multiple phase reclamation projects [9]. However, there is a strong correlation between the degree of soil consolidation and completion time of the land reclamation project [10]. Significant differences in surface deformation have been observed in reclaimed areas completed at different time points. For example, surface

deformation in the early reclaimed areas of Xiamen Airport shows relative stability [11]. The artificial reclamation area of Shanghai's Chongming Island expanded from west to east, and the surface subsidence rate also showed a trend of gradually increasing from west to east [12]. Shanghai Lingang New City completed in 1973 exhibits excellent surface stability, while significant deformation occurred in completed reclamation projects after 2002 [13].

At the same time, Tianjin reclamation is an important industrial zone and the maritime gateway of the national shipping centre in North China. A large number of factories, ports, and buildings are constructed on the surface. The continuous load of surface structures provides a good foundation for the development of land settlement. Additional load from buildings is one of the factors causing land subsidence in urban areas [14,15]. The buildings in the industrial zone of Wuhan are densely constructed, resulting in a substantial surface load and significant ground settlement [16]. Due to artificial reclamation area at Shanghai Pudong Airport, surface deformation is greater in areas where large quantities of goods are stockpiled [17]. Under combined effects of soil consolidation and surface building load, land subsidence in Tianjin Binhai New Area is inevitable. However, land subsidence is difficult to recover, and it can give rise to secondary hazards such as coastal erosion [18], seawater intrusion [19], and soil salinization [20,21]. Additionally, it elevates the risk of instability for artificial structures, undermines the stability of infrastructure like roads, railways, buildings, dams [22], and submarine tunnels, ultimately reducing their service lifespan. Therefore, it is of great significance to determine the extent of surface deformation in reclamation lands completed at various times and analyze the surface deformation characteristics of different land-use types. These efforts are crucial for effectively preventing and controlling land subsidence hazards, ensuring the structural safety of buildings, and informing the planning and design of future surface constructions in the subsequent phases of land reclamation in Tianjin Binhai New Area.

Currently, research conducted by domestic and international scholars on Tianjin primarily focuses on the surface deformation characteristics within the main urban area [23], the long time series of groundwater level changes [24,25], and the response relationship between surface deformation and groundwater level changes [26,27], which is important for the development of land resources and ensuring the safety of infrastructure in Tianjin. However, groundwater exploitation has not been carried out in the reclaimed areas of Tianjin Binhai New Area. The existing settlement analysis of the urban area cannot explain the settlement characteristics of the Binhai New Area; meanwhile, the differences in ground deformation between reclamation completion time and different land-use types are not analyzed in depth. In order to provide a basis for the settlement management and engineering control measures, it is particularly urgent to further investigate the settlement driver factor in Binhai New Area.

In large-scale artificial reclamation in Tianjin Binhai New Area, traditional surface deformation measurement methods such as Leveling, GNSS, Borehole Extensometers, and Tilt measurement can obtain high-precision surface deformation, but they are all point-based measurements, and it is difficult to acquire high-precision spatially continuous large-scale deformation when using them. In addition, the cost is high [28]. In recent years, with the development of synthetic aperture radar interferometry technology, time series InSAR is widely used in surface deformation detection with high precision, large scale, and low cost. Compared to PS-InSAR, SBAS-InSAR has good surface deformation detection capability in areas where man-made structures are sparse and lack sufficiently stable scatterers.Therefore, PS-InSAR is typically utilized in urban areas, while SBAS-InSAR is predominantly applied in suburban regions [16,29–32].

In summary, the artificial reclamation land in Tianjin Binhai New Area has a significant risk of ground subsidence. Currently, there is no exploration of surface deformation patterns in the reclamation area, which fails to meet the requirement of disaster prevention and later land resource development in the reclamation area. High-precision SBAS-InSAR is employed to detect the spatio-temporal deformatio; Landsat-5, Landsat-7 and Landsat-8 from 1995 to 2022 are used to acquire coastline changes; and GF-1 and GF-2 from 2018

to 2022 are used to identify land-use types of reclamation in Tianjin Binhai New Area. Combined with the reclamation projects time and land-use types, the driving factor of surface deformation can be analyzed. This has important practical significance for ensuring the safety of infrastructure, preventing geological disasters, and planning the design of artificial reclamation in Binhai New Area.

2. Study Area

Tianjin Binhai New Area is located in the northwestern part of Bohai Bay. The geomorphology consists of an intertidal plain and a marine low plain. The coastline is low and straight, the elevation gradually decreases from west to east [33]. The main geological formation is made up of unconsolidated Quaternary and Upper Neogene deposits [34]. The Quaternary sediments primarily consist of alluvial and marine deposits [35]. Coastal sediments are widely distributed on the surface and consist mainly of silty clay and loamy clay with significant porosity and high moisture content. These sediments generally manifest soft plasticity and low strength [36].

According to "Urban Master Plan of Binhai New Area", the total area of reclamation in Binhai New Area reached 413.6 km^2 in 2020. A significant number of ports, factories, petrochemical plants, residential buildings, and grain and oil refining plants have been constructed in the reclaimed area. These facilities facilitate the transshipment and transportation of bulk goods such as containers, crude oil, minerals, and coal. Furthermore, the area serves as a crucial marine gateway for the North China Plain [37], holding a significant strategic position. The reclamation land of Binhai New Area can be divided into the Nangang Industries Zone, the Lingang Industrial Zone, and Hangu Port in Figure 1. The Nangang Industries Zone is the largest reclamation port [38] and the Lingang Industrial zone is the maximal comprehensive trade port in northern China.

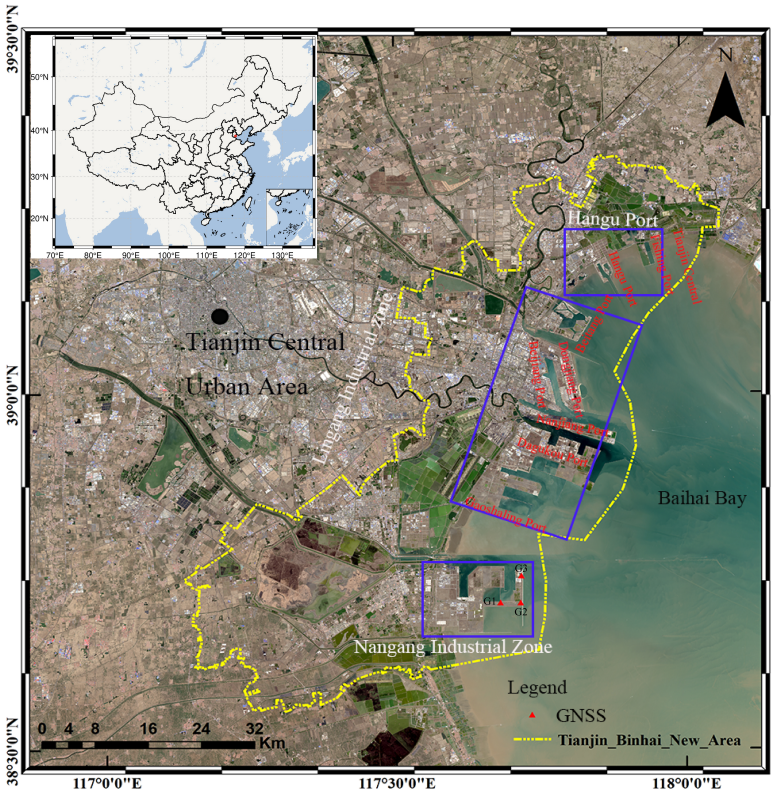

Figure 1. The location of the Nangang Industrial Zone, the Lingang Industrial Zone and Hangu Port in Tianjin Binhai New Area. The red triangles represent the locations of the GNSS ground monitoring points.

3. Data and Methodology

3.1. Datasets

We note that the study area is only covered by Sentinel-1A ascending images from 2017 through 2022. A total of 159 ascending Sentinel-1A Single Look Complex (SLC) images from 3 January 2017 to 27 December 2022 were obtained to monitor ground deformation characteristics and spatial distribution in the reclamation area of Tianjin Binhai New Area. The parameters are shown in Table 1.

Table 1. Basic parameters of Sentinel-1A.

Parameters	Description
Orbit direction	Ascending
Track	69
Band	C
Wavelength (cm)	5.6
Incidence angle (°)	36.14
Azimuth and Range resolution (m)	5 × 20
Temporal coverage	3 January 2017–27 December 2022
Revisit time (day)	12
Number of images	159

Landsat5, Landsat7, Landsat8 images from 1995 to 2022 were applied to identify coastline changes; GF-1 and GF-2 from 2018 to 2022 were used to identify land-use types.The information of the acquired image data set is shown in Table 2.

Table 2. The parameters of the Optical images data set.

Image	Temporal Coverage (Year)	Number of Images	Resolution (m)	Purpose
Landsat-5	1995–2011	35	30	Coastline Change Identification
Landsat-7	2012	5	30	Coastline Change Identification
Landsat-8	2013–2022	29	30	Coastline Change Identification
GF-1	2019–2022	23	2	Land-Use Type Identification
GF-2	2018–2019	4	0.8	Land-Use Type Identification

3.2. Methodology

Tianjin Binhai New Area has a large area of bare land. Currently, reclamation initiatives within the Nangang Industrial Zone, Dagukou Port, and Hangu Harbor are ongoing. However, these ongoing projects pose challenges in terms of obtaining a substantial number of stable scatterers necessary for accurate measurement. Therefore, to capture ground deformation accurately, we employed the Synthetic Aperture Radar (SAR) interferometry technique known as a Small Baseline Subset (SBAS-InSAR). The principle of SBAS-InSAR is to divide all SAR images obtained in the same area into several small subsets that satisfy the requirements of both temporal and spatial baselines [39–41]. The

least squares method was used to solve the phase in each set, and then the remaining small baseline sets were combined. Singular Value Decomposition (SVD) was used to slove multiple small baseline sets to obtain the least squares solution under the smallest norm and then obtain the time series deformation sequence in the study area [42–44]. However, SBAS-derived displacements were in the LOS direction; therefore, LOS measurements d_{LOS} were converted into a vertical direction D_v according to the following incidence angle θ:

$$d_V = \frac{d_{LOS}}{\cos\theta}. \quad (1)$$

To avoid temporal and spatial decorrelation, the time baseline threshold of 60 days and the spatial baseline threshold of 190 m were set [12]. A total of 710 image pairs were generated, of which 164 image pairs with poor interferences were deleted and 537 image pairs were used for surface deformation extraction from January 2017 to December 2022, as shown in Figure 2. Multi-viewing vlues with the azimuth looks and range looks were 5 and 1, and Goldstein filtering was applied for noise removal [45]. The coherence threshold was set to 0.3 [12]. The Shuttle Radar Topography Mission digital elevation model with a resolution of 30 m was used to remove topography phase. Precise Obit Data (POD) provided by the European Space Agency (ESA) (https://scihub.copernicus.eu/gnss/#/home) were used to remove orbit error. The Delaunay MCF method was used for phase unwrapping. Atmospheric phase removal by high-pass temporal filtering and low-pass spatial filtering was also used [12,44,46].

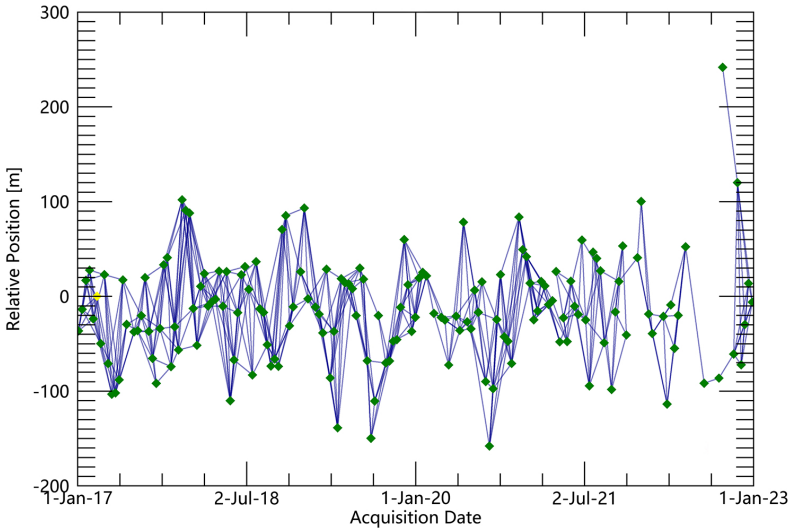

Figure 2. Interferometric pairs formed by Sentinel-1A data sets. The green squares and blue lines represent the image and interferometric pairs, respectively. The yellow dot refers to the super master image.

Geometric and atmospheric corrections were applied to the optical images in Table 2. Landsat-5, Landsat-7, Landsat-8 from 1995 to 2022 were used for identify coastline change by visual interpretation. Firstly, surface construction types were obtained by visual interpretation of GF-1, GF-2; then, the interpretation results were corrected by using high-precision electronic maps and Google Earth; finally, the surface construction types were confirmed by field investigation. The results showed that the accuracy of the interpretation reached 99%.

4. Results and Disscussion

4.1. SBAS-InSAR Results and Validation

Ground deformation in Tianjin Binhai New Area from 3 January 2017 to 27 December 2022 was extracted, as shown in Figure 3. Significant spatial variation was observed in surface deformation. In the offshore direction, all the artificial reclamation areas showed a trend of gradual increase in surface deformation. The maximum deformation near the

land in the Nangang Industrial Zone was −50 mm, while the maximum settlement in the offshore area was −890 mm. In the direction of expansion along the coastline, the subsidence in Lingang Industrial Zone changed from 45 mm to −580 mm. The maximum surface deformation in the nearshore area of Hangu Port was −140 mm, while the surface deformation in the offshore area was −290 mm.

Additionally, less surface deformation information was obtained in Figure 3 marked by the black dashed rectangle. Figure 5 reveals these areas of red rectangular marked area in (f) that experienced seawater intrusion after completion of the reclamation project. The reclaimed area's soil was eroded by seawater, resulting in surface water infiltration. A multi-phase reclamation project was taken in these areas, leading to less land deformation information observed in Figure 3.

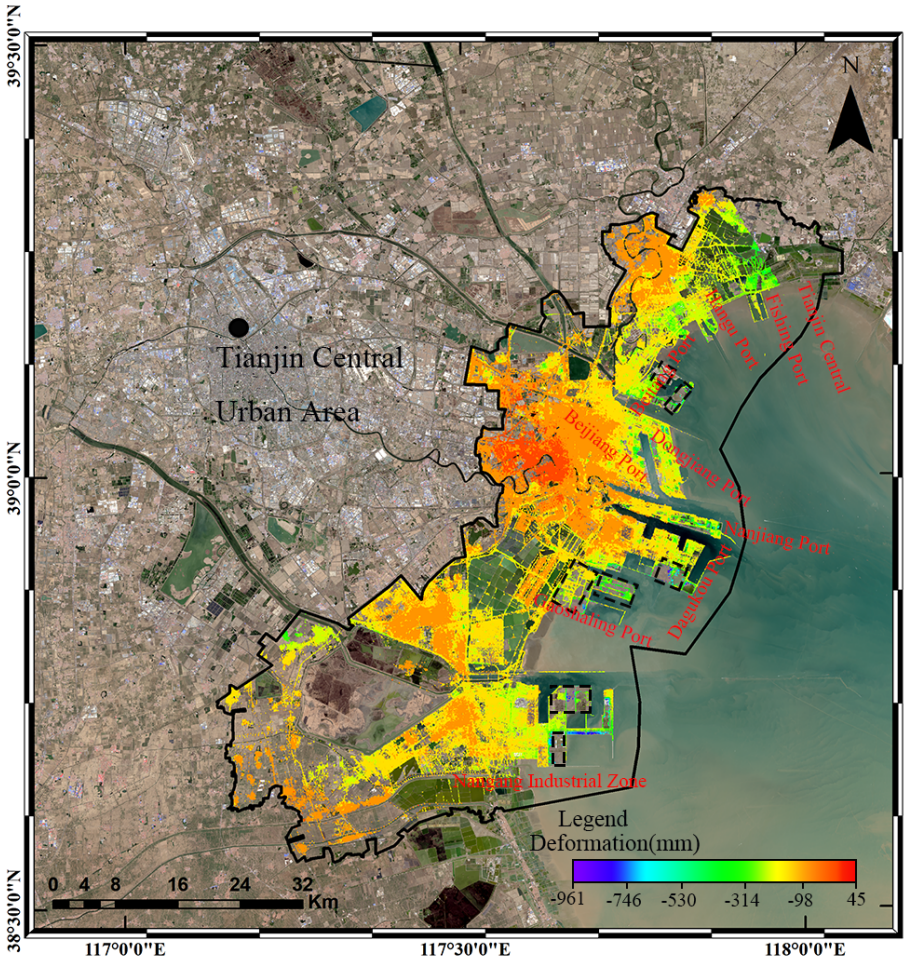

Figure 3. SBAS-InSAR deformation results.

Data of a total of three ground GNSS monitoring stations were collected, and these stations are located in the Nangang Industrial Zone of Tianjin Binhai New Area, as indicated by the red triangles in Figure 1. The data for monitoring station G1 cover the period from 24 March 2020 to 10 September 2022. The data for G2 span from 23 May 2020 to 15 December 2022. The monitoring period for G3 is from 24 March 2020 to 25 May 2022. To quantitatively evaluate the accuracy of ground deformation obtained by SBAS-InSAR, this study conducted a comparsion between the SBAS-InSAR with GNSS measurements, as shown in Figure 4. The root mean square errors (RMSE) for points G1–G3 are 5.253 mm, 5.614 mm, and 4.936 mm, respectively.

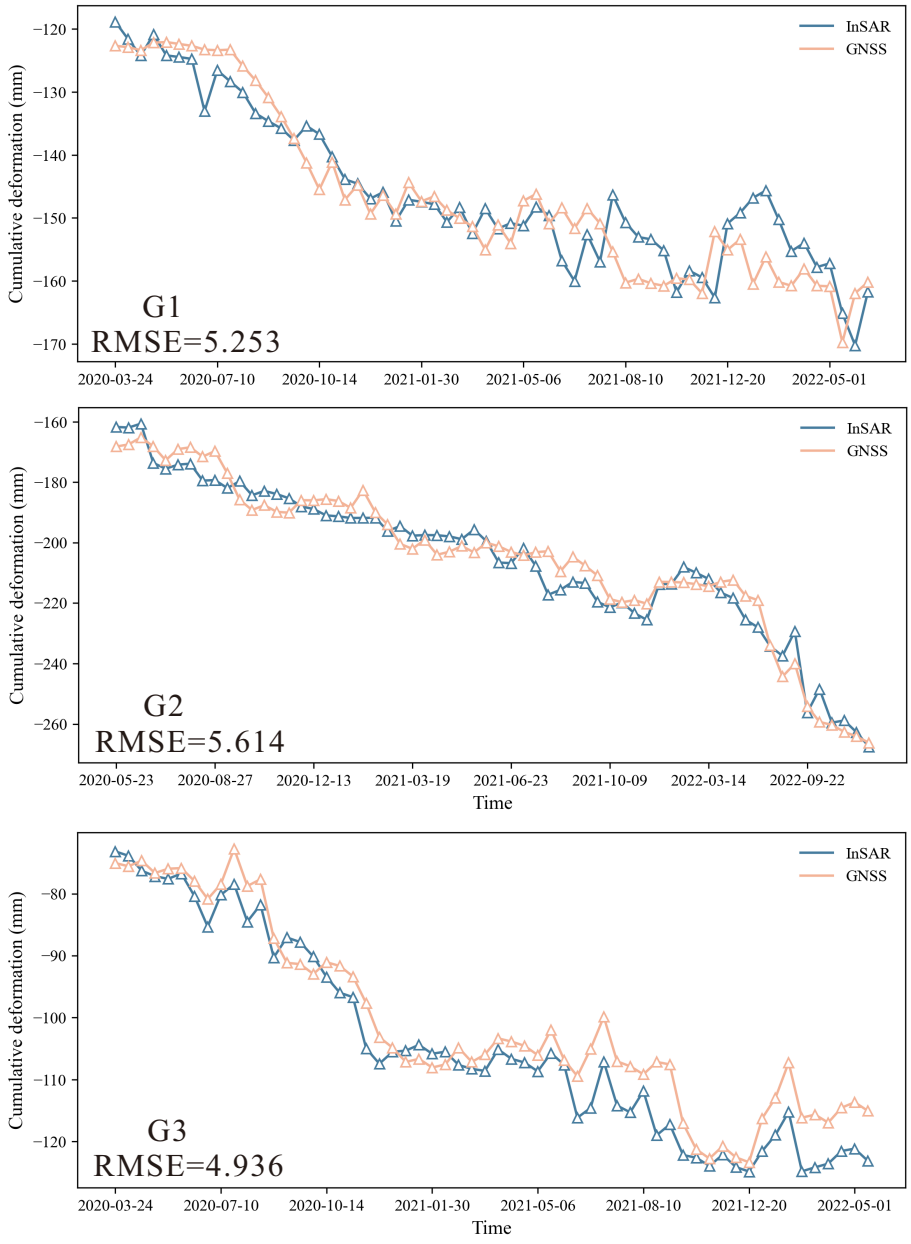

Figure 4. Comparison between SBAS-InSAR and GNSS results.

4.2. Land Reclamation Spatial Evolution at Tianjin Binhai New Area

Figure 5 shows the spatial evolution history of land reclamation in Tianjin Binhai New Area. In Figure 6, reclamation in the Lingang Industrial Zone started at the earliest time, with Beijiang Port completed in 1995, while all ports in the Lingang Industrial Zone, except Gaoshaling Port, were completed in 2014. The reclamation project in the Nangang Industrial Zone began in 2009 and was mostly completed by 2022. Hangu Port's reclamation started in 2009 and was completed in 2014, while Tianjin Central Fishing Port was still under construction in 2022.

The reclamation area for each time point was calculated. The results are shown in Figure 7. It can be observed that the artificial reclamation acreage was relatively large in 2009, 2010, and 2014, with 56.265 km^2, 61.441 km^2, and 56.548 km^2, respectively. The artificial reclamation area gradually increased from 1995 to 2010 and reached a peak in 2010. From 2015 to 2022, the artificial reclamation area significantly decreased, indicating a recent decline of land reclamation activities in Tianjin Binhai New Area.

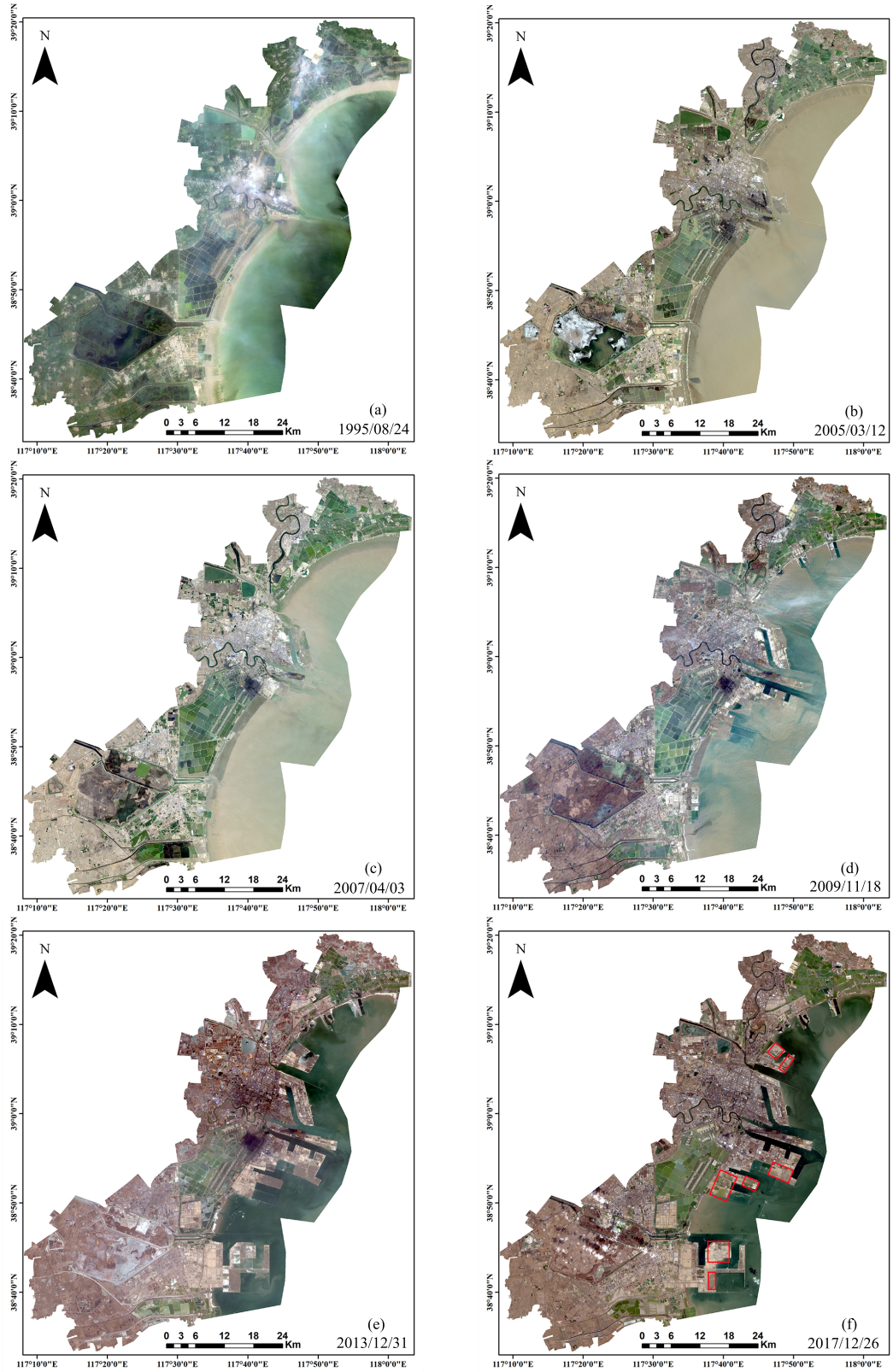

Figure 5. Spatial Evolution of Tianjin Binhai New Area Land Reclamation. The background image obtained from Landsat-5 and Landsat-8 satellites.

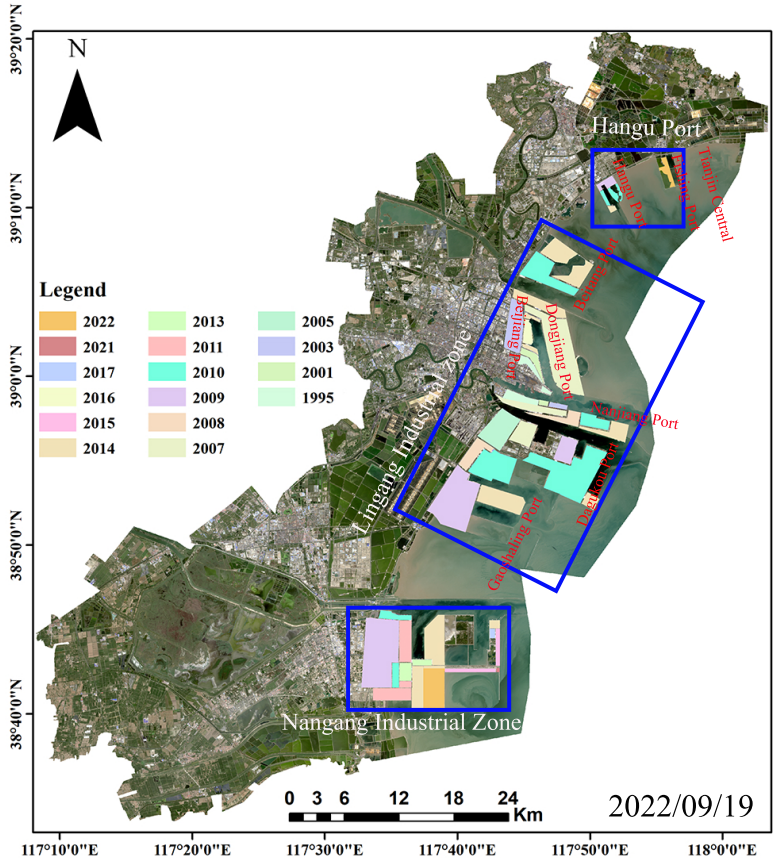

Figure 6. Statistical map of the spatial and temporal evolution of reclamation areas.

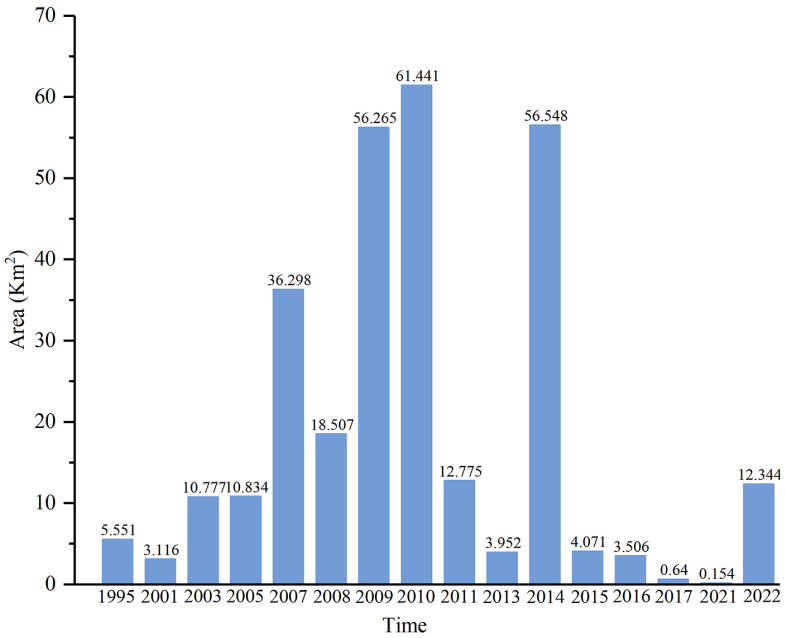

Figure 7. Reclamation area of Tianjin Binhai New Area.

4.3. Responsive Relationship between Reclamation Time and Surface Deformation

Figure 8 provides an amplified view of surface deformation of the Nangang Industrial Zone, the Lingang Industrial Zone and Hangu Port. The blue dashed rectangle in Figure 8a experienced the most severe surface deformation, with a maximum surface deformation value of −890 mm, the reclamation of which was completed in 2015. There was a significant spatial difference of surface deformation in the Nangang Industrial Zone, with a trend of

severe subsidence from land to Bohai Bay. In the reclamation completed in 2009, the surface deformation was around −98 mm, significantly smaller than that in the area completed at a later stage.

In Figure 8b, it can be seen that the surface deformation in the Lingang Industrial Zone gradually intensified from the land to the marine area, and there was a significant difference in surface deformation along the coastline extension. The deformation in the area near the land ranged from 45 mm to −98 mm, while the settlement of the surface near the marine area was in a range from −98 mm to −580 mm. The areas completed in 2010 and 2014 exhibited much greater subsidence compared to those completed at other times.

In Figure 8c, it can be seen that the ground deformation of the Hangu Port land reclamations completed in 2009 and 2010 were −140 mm to −160 mm, and −178 mm to −290 mm, respectively. Tianjin Central Fishing Port is still under construction.

Additionally, the reclamation projects in the Nangang Industrial Zone and Hangu Port were conducted later than those in the Lingang Industrial Zone; as a result, the surface settlement in most areas of Nangang and Hangu port are larger than those in the Lingang Industrial Zone.

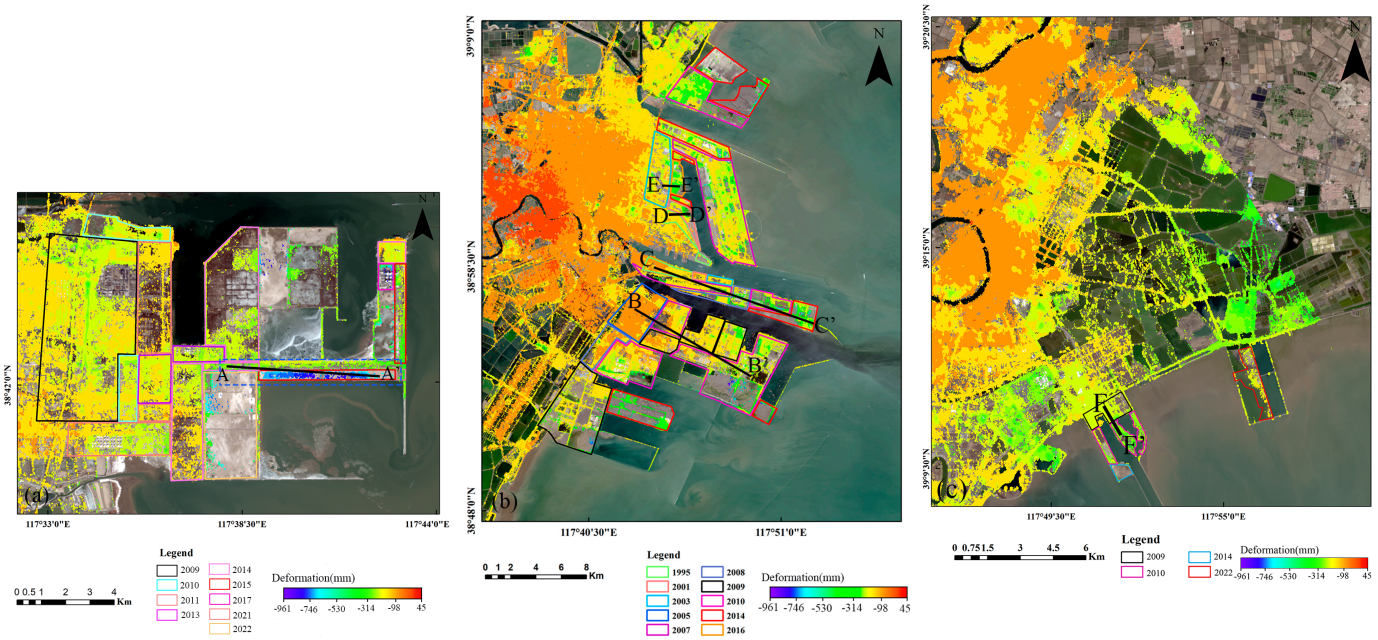

Figure 8. Ground deformation rate map. (**a**) Nangang Industrial Zone. (**b**) Lingang Industrial Zone. (**c**) Hangu Port.

Comparing the magnitudes of surface deformation and reclamation time in each area, it becomes evident that there is a high correlation between surface deformation and reclamation time. To quantify the differences in surface deformation among the reclamation areas completed at different time points, the cumulative surface deformation from January 2017 to December 2022 was extracted for the six black solid lines indicated in Figure 8. The results are shown in Figure 9.

Figure 9 demonstrates the quantitative relationship between different land reclamation periods and surface deformation. Different background colors represent different completion times of land reclamation. Multiple surface subsidence funnels are observed in the areas where the six profile lines, with significant differences in subsidence magnitudes among different regions.

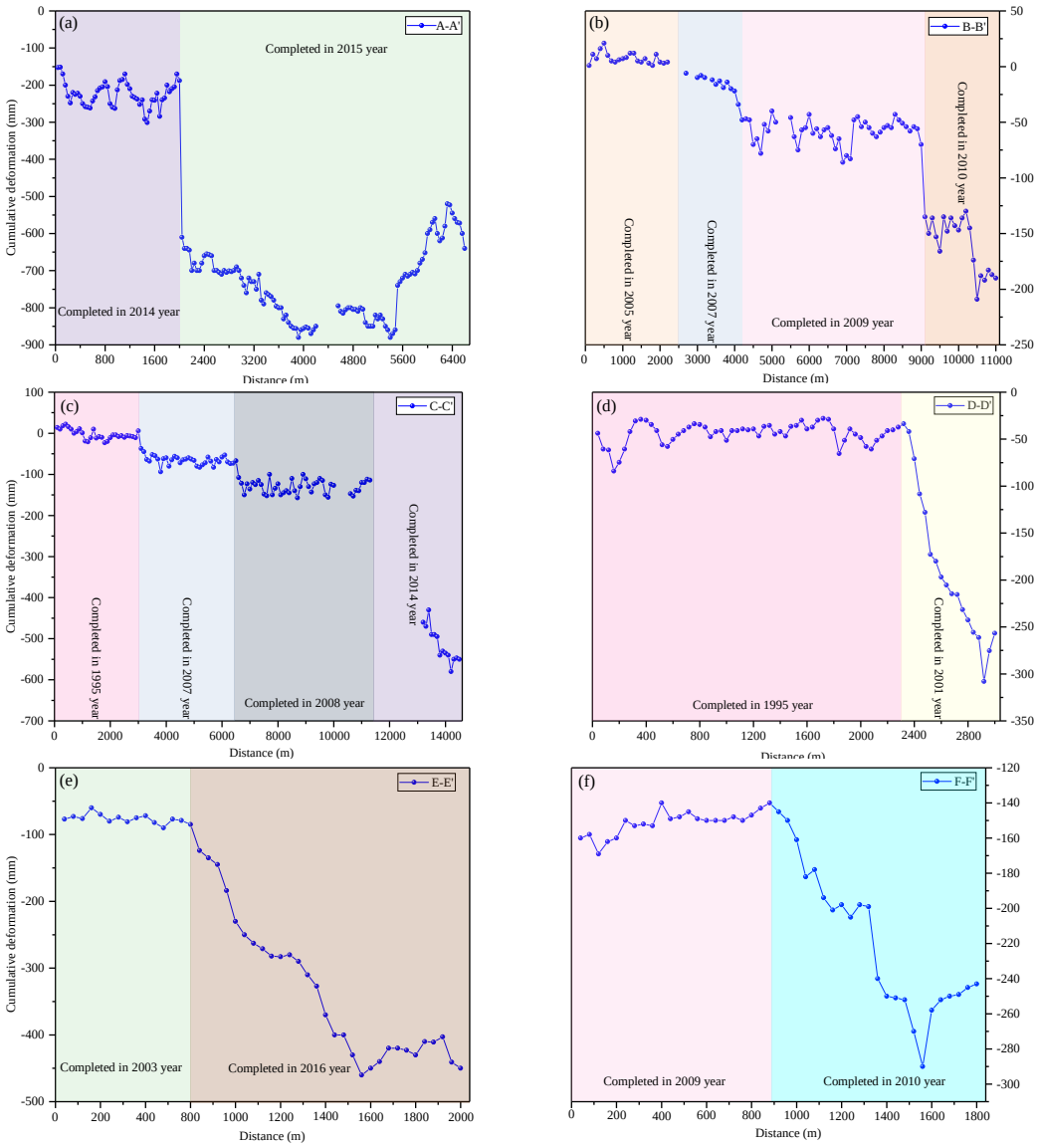

Figure 9. Cumulative deformation of Tianjin Binhai New Area along six profiles form January 2017 to December 2022; their positions are marked in Figure 8. (**a**) Profile A-A′; (**b**) Profile B-B′; (**c**) Profile C-C′; (**d**) Profile D-D′; (**e**) Profile E-E′; (**f**) Profile F-F′.

In Profile A-A′, the surface deformation in the reclamation area completed in 2014 ranges from −152 mm to −301 mm, and the most severe surface deformation was completed in 2015, ranging from −610 mm to −890 mm. In Profile B-B′, ground deformation in the reclamation area completed in 2005, 2007, 2009 and 2010 ranges from 1 mm to 22 mm, −8 mm to −48 mm, −50 mm to −86 mm and −130 mm to −209 mm, respectively. In Profile C-C′, the surface deformation in the reclamation area completed in 1995 ranges from 1 mm to −12 mm, while in 2007, it ranges from −37 mm to −94 mm, in 2008 it ranges from −105 mm to −152 mm, and in 2014 it ranges from −460 mm to −550 mm. In Profile D-D′, the surface settlement in the reclamation area completed in 1995 ranges from −31 mm to −70 mm, and in 2001 it ranges from −76 mm to −330 mm. In Profile E-E′, the ground subsidence in the reclamation land was completed in 2003, ranging from −60 mm to −90 mm, while in 2016, it ranges from −124 mm to −460 mm. In Profile F-F′, the ground settlement of artificial reclamation land completed in 2009 and 2010 are −140 mm to −160mm, and −178 mm to −290 mm, respectively.

To further reveal the surface deformation patterns of the reclaimed land, this study extracted time series deformation of four points (P1–P4) shown in Figure 10, and the

location is in Figure 11. Among them, P1–P4 are located in bare land. From Figure 10, it can be seen that the surface cumulative deformation for the bare land reclaimed in 2007, 2010, 2014, and 2015 were −40 mm, −201 mm, −281 mm, and −871 mm, respectively, indicating a significant trend of severe surface deformation in the areas where reclamation was completed later. Although the bare land areas in Tianjin Binhai New Area were not developed, the fill soil itself causes consolidation, and the dredged soil as a large-scale load causes compression deformation in the underlying layers. The weak soil layer also experiences secondary consolidation under the long-term loading of the fill soil [47], resulting in significant settlement in the bare land areas of the study area. The cumulative deformation at Point P2 is greater than it is at Point P3. However, in 2020, there was an acceleration of deformation at Point P2, resulting in significantly higher deformation at Point P2 compared to that at Point P3 after 2020. According to the comparative analysis of optical images of Points P2 and P3 in 2020, it is evident that in 2019, the area near Point P2 underwent ground leveling and drainage towards the area where Point P2 is located. This led to water seepage on the surface at Point P2, while no seepage was observed at Point P3. Surface water accumulation can affect surface stability and cause settlement, which is consistent with the surface deformation trend indicated by the blue dashed rectangular box in Figure 8 of the Nangang Industrial Zone.

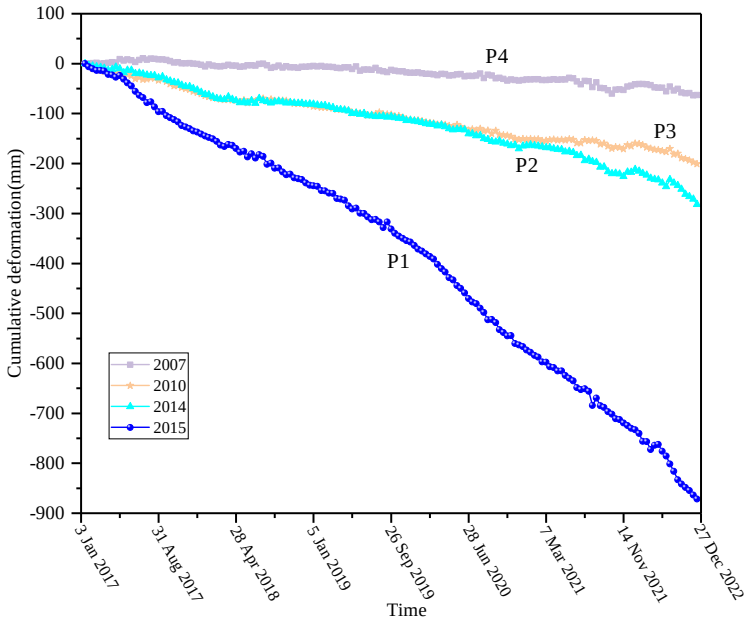

Figure 10. Bare land time series deformation.

All six profiles of cumulative deformation and the time series deformation of the bare land further demonstrate a strong correlation between surface subsidence and the time of reclamation. The earlier the reclamation project is completed, the more stable the consolidation of the fill and the compression of the underlying soil layer, resulting in lesser surface subsidence. Conversely,the severe land subsidence occurred over newly reclaimed areas. A similar phenomenon was observed in the reclamation land of Xiamen new airport [11].

At the same time, in Figure 9a,c, the surface settlement for the areas reclaimed in 2014 are −152 mm to −301 mm, and −460 mm to −550 mm, respectively. In Figure 9c,d, the surface deformations for the areas reclaimed in 1995 are 1 mm to 22 mm and −31 mm to −70 mm. In Figure 9b,c, the surface subsidences of reclamation completed in 2007 are −8 mm to −48 mm and −37 mm to −94 mm, respectively. Figure 9b,f demonstrate reclamation completed in 2009; the ground deformations are −30 mm to −98 mm, −140 mm to −160 mm, respectively. This indicates significant variations in surface deformation among reclamation areas completed at the same times in different regions.

4.4. Relationship between Land-Use Types and Deformation

In order to investigate the spatial differences in ground settlement for reclamation completed at the same time, GF-1 and GF-2 images were used to identify the land-use types by visual interpretation. The land-use types were as shown in Figure 11. From Figure 11, it can be observed that the main land-use types in the reclamation areas are petrochemical plants, industrial areas, residential areas, cargo storage areas, and mineral storage areas. The unmarked reclamation areas are bare land. A higher degree of industrialisation is observed in the Lingang Industrial Zone, with a larger number of factories and cargo storage areas. The land-use types of the Nangang Industrial Zone are bare land, petrochemical plants, factories and mineral storage areas. The Hangu Port reclamation area has very few factories.

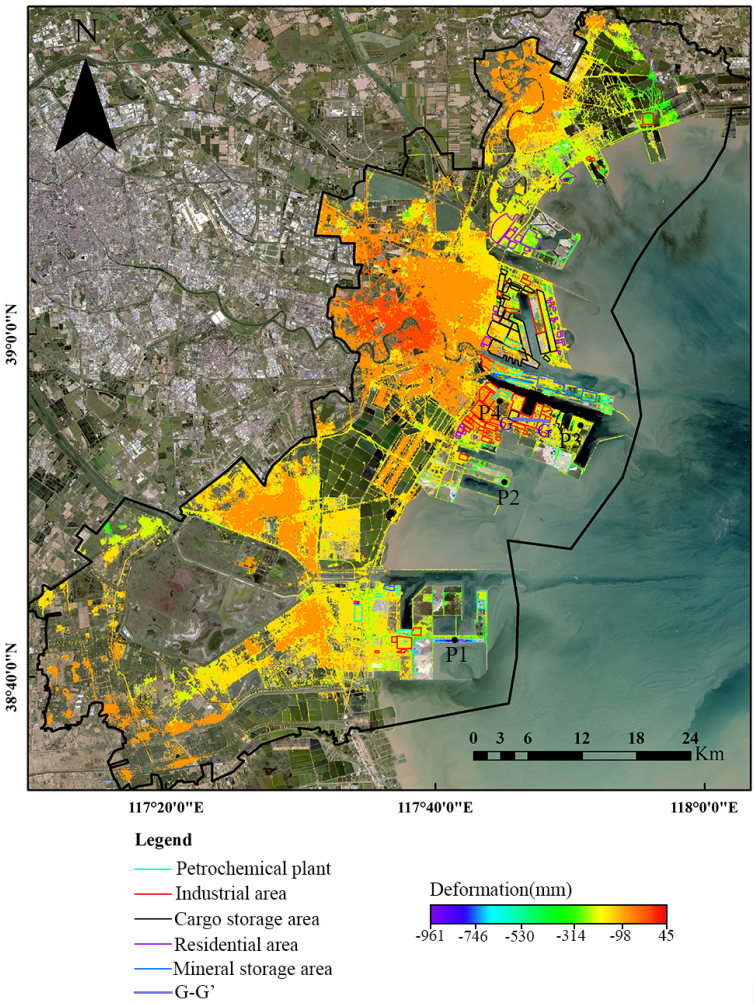

Figure 11. The deformation of surface construction type, with different-color solid boxes representing different surface construction types. The black points are the sampling points for extract time series deformation. Points P1–P4 are bare land, and the reclamation times are 2015, 2014, 2010, and 2007, respectively.

According to Figure 9, significant differences in surface deformation were observed in the reclamation areas completed at the same time. In Figure 11, the land-use types in the reclamation area completed in 1995 along profile lines C-C′ and D-D′ in Figure 9 are factories and cargo storage areas. The cargo storage area on profile line E-E′ includes the Chihaikia Car Ro-Ro Terminal and the Tianjin Maoxin Storage Yard. Due to long-term static load from bulk cargo storage and dynamic load from transportation of goods such as vehicles, the subsidence of the cargo storage area is greater than that of the factory area. In Figure 9, for profile line B-B′, for which the reclamation area was completed in 2007, the

surface subsidence is smaller compared to that id C-C′. According to Figure 11, the surface construction types along profile lines B-B′ and C-C′ are bare land and mineral storage area, respectively. The mineral storage area has a large amount of mineral piles on the surface, which imposes a large surface load. Additionally, the bare land on profile line B-B′ was reclaimed earlier, and its surface deformation is relatively stable.

Combining the surface deformation characteristics of different construction types in Figures 9 and 11, it can be concluded that the land-use types is the main reason for the significant difference in the deformation of reclamation areas completed at the same time. To further analyze the differences in surface deformation in the reclamation areas completed during the same period, we extracted the deformation profile at the location of G-G′ in Figure 11. It is shown in Figure 12.

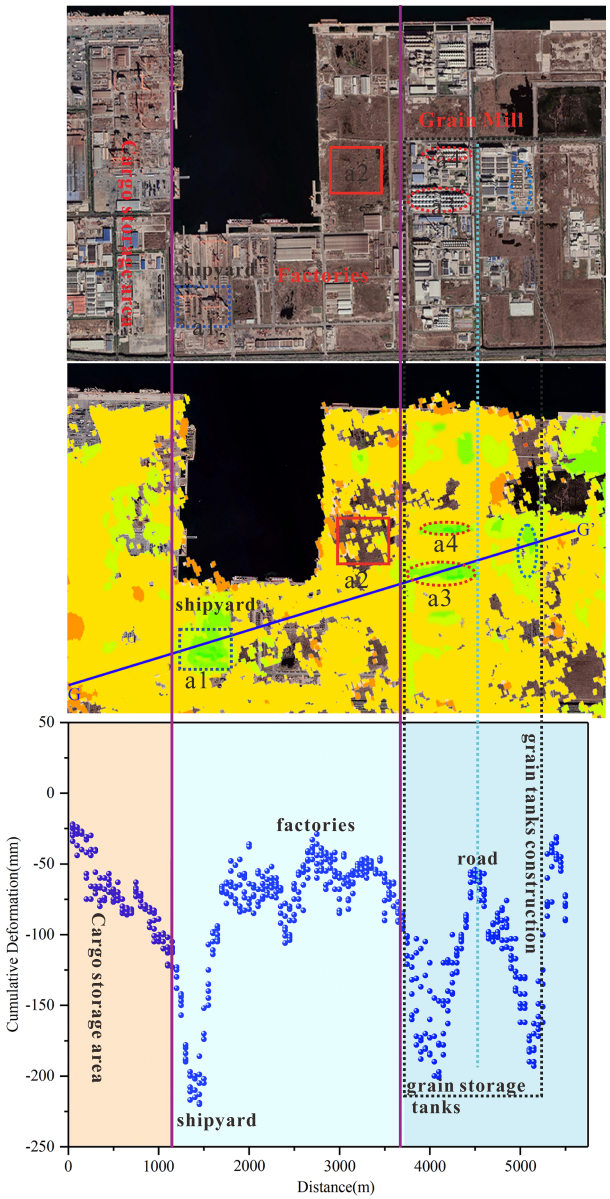

Figure 12. Cumulative deformation of the Lingang Industrial Zone along G-G′ profiles form January 2017 to December 2022, whose positions are marked in Figure 11. (a1) Heavy shipyard, (a2) bare ground, (a3) 67 grain storage tanks and (a4) 27 storage tanks.

According to Figure 12, there is a subsidence funnel with a maximum subsidence of −220 mm in the blue dashed rectangle, which is Lingang shipyard and China Shipbuilding (Tianjin) Ship Manufacturing Co., Ltd. It can be seen from the optical image that a crane is

located in the blue dashed rectangle area for large-scale ship movement and assembly; the surface load is large. In the factory zone, the surface deformation is relatively minor. This is due to the fact that the factory occupies a large area and has sparse building distribution, resulting in a dispersed surface load. The black dashed rectangle represents Jingliang (Tianjin) Grain and Oil Industry Co., Ltd., which has two grain and oil plants. The two subsidence funnels align with the locations of the plants. In the surface deformation map, the red dashed elliptical area shows significant surface deformation, and from the optical image, it can be seen that two grain storage tanks are placed in these elliptical areas, creating a high and concentrated surface load. The cyan dashed elliptical area represents the ongoing construction of grain storage tanks, higher anthropomorphic disturbances resulting in severe surface settlement. The cyan dashed line is located at the intersection of the subsidence funnels of the grain plants, showing relatively small surface deformation. Based on the optical image, this area corresponds to a road, with a smaller surface load compared to that of the area where the grain storage tanks are located. The surface subsidence in the cargo storage area ranges from −75 mm to −90 mm. It can be observed from the optical image that this area belongs to a logistics company, but the number of containers is small. Based on the above information, it can be concluded that significant subsidence occurs in areas with high surface load.

In Figure 12, a1 is located in the heavy shipyard, a2 is bare land without any buildings, and there is no surface water seepage phenomenon observed in area a2 based on the data from the optical image. Both a3 and a4 are located at the grain storage tanks; the numbers are 67 and 27, respectively, and judgind from optical image specification, the size of the storage tanks is the same. To compare the surface deformation characteristics under different surface loads, this study randomly and uniformly selected 20 points from locations a1–a4 and the road to extract the average surface settlement. The result is shown in Figure 13.

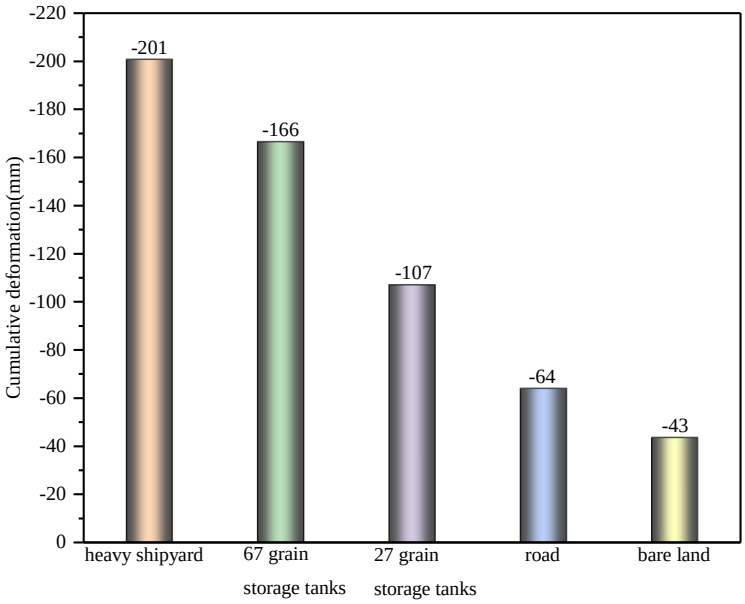

Figure 13. Average ground settlement for different land-use types with reclamation completed at the same time.

From Figure 13, it can be seen that the average surface settlement gradually decreases in the five areas. The average settlement in the heavy shipyard area is the largest with −201 mm. A large amount of steel for shipbuilding is piled up in the area, and a large number of cranes was built on the surface for assembling ships, which can be regarded as the cause of a great surface load in this area. In the two grain and oil tank areas, the surface load in the area with 67 tanks is greater than that in the area with 27 tanks, with average settlements of −166 mm and −107 mm, respectively. The road is a necessary route

for the grain and oil transportation of Beijing Grain (Tianjin) Industry Co., Ltd., and there are many vehicles. However, the surface load is much smaller than that of the grain storage tank areas and the heavy shipyard, with an average settlement of −64 mm. The bare land area is undeveloped with no surface loading and an average surface settlement of −43 mm. Combining the surface load and surface settlement in these five areas, it can be observed that there is a positive correlation between surface load and surface settlement. The greater the surface load, the larger the surface settlement.

In summary, different land-use types lead to significant differences in surface deformation of the reclaimed area completed at the same time. In order to ensure the safety of buildings in the reclaimed area, intensive monitoring should be carried out for heavy industrial areas with large surface loads. When developing and utilizing reclaimed areas, heavy plants should be planned to avoid areas of serious surface settlement, and foundations should be compacted and reinforced before construction.

4.5. Disscussion

Surface deformation caused by the overexploitation of groundwater in Tianjin was first observed in 1959 [23]. From 1959 to 2008, the maximum cumulative surface subsidence in Tianjin reached 3.2 m [48]. At the same time, in the early 1980, the implementation of the Luanhe–Tianjin Water Diversion Project [49] and the comprehensive water diversion of the South-to-North Water Transfer Project in 2014 significantly alleviated the trend of groundwater depletion in Tianjin City [50,51]. The surface in the central urban area of Tianjin is relatively stable, with the subsidence funnel shifting from the central urban area towards the suburbs [8]. Intensive heavy load surface construction and over-exploitation of groundwater by industrial production are the main causes of surface deformation in suburban areas [47,49]. Thus, it can be seen that the main causes of surface settlement in Tianjin are groundwater exploitation and surface building loads. There is no groundwater extraction in the reclaimed area of Tianjin Binhai New Area, and dredger fill soil has the characteristics of high water content, high porosity, and low strength, which is very prone to surface subsidence. The reclaimed area of Tianjin Binhai New Area is an important land resource in Tianjin, which is of great significance to the economic development of Tianjin. This paper used SBAS-InSAR to identify the spatial and temporal distribution characteristics of surface settlement in the current reclamation area of Tianjin Binhai New Area. The differences in surface deformation of reclaimed areas at different reclamation times were analyzed with optical images, and the deformation characteristics of reclaimed areas under different building types and loads were investigated. This paper is of great practical significance to the development and utilization of the reclaimed area and the prevention and control of geologic hazards in later stages.

In this study, the surface deformation characteristics of the artificial reclamation land in Tianjin Binhai New Area from 2017 to 2022 were obtained using SBAS-InSAR, and LOS deformation was converted to vertical deformation based on the incidence angle of Sentinel-1A. However, when converting LOS deformation to vertical deformation, the influence of horizontal deformation was ignored, which may lead to overestimation or underestimation of the vertical deformation [52]. In Figure 4, the GNSS monitoring values are consistent with the obtained SBAS-InSAR vertical deformation trend, with REMS values at points G1–G3 being 5.253, 5.614, and 4.936, respectively. However, the maximum deformation errors between GNSS and SBAS-InSAR at points G1–G3 were 10 mm, 11 mm, and 14 mm, respectively, which may have been caused by the ignored horizontal deformation.

5. Conclusions

In order to satisfy the requirement of disaster prevention and control in the reclaimed area of Tianjin Binhai New Area and the rational development of land resources in the later stage, the SBAS-InSAR method was employed to process 159 ascending Sentinel-1A pieces of data from 2017 to 2022, and surface deformation was detected. In total, 69 scenes of Landsat-5, Landsat-7, and Landsat-8 images from 1995 to 2022 were used to interpret

the land reclamation process. GF-1 and GF-2 data from 2018 to 2022 were interpreted to obtain the main land-use types, and the types were determined to be Petrochemical plant, Industrial area, Residential area, Cargo storage area, Mineral storage area and Bare land in the reclaimed land of Tianjin Binhai New Area. Combining the surface deformation data obtained by SBAS-InSAR with the reclamation process and land-use types, the article draws the following conclusions:

The artificial reclamation acreage increased from 1995 to 2010, reaching a peak of 61.441 km^2 in 2010. The artificial reclamation area significantly decreased from 2015 to 2022, indicating a slow expansion of the reclamation area in recent years.

In the offshore direction, the maximum surface deformations of the reclamation land in the Lingang Industrial Zone, the Nangang Industrial Zone and Hangu Port were 45 mm to −580 mm, −98 mm to −890 mm, and −140 mm to −290 mm, respectively. This indicates a strong correlation between surface settlement and reclamation time, with newly completed land reclamation areas showing severe surface deformation. For new developments in the field of land reclamation, careful consideration should be given to the scale and type of buildings.

The average surface subsidence of heavy shipyards, the area with 67 grain storage tanks, the area with 27 grain storage tanks, road, and bare land were −201 mm, −166 mm, −107 mm, −64 mm, and −43 mm, respectively. This indicates that there is a positive correlation between surface load and surface subsidence, and the larger the surface load, the ore severe the surface subsidence.

Author Contributions: Y.C. and F.Y. conceived the manuscript, Y.C. performed the experiments, interpreted the results and drafted the manuscript. Y.C., X.F. and J.C. contributed to the discussion of the results. All authors conceived the study, and reviewed and approved the manuscript. All authors have read and agreed to the published version of the manuscript.

Funding: This research was supported by the National Key Research and Development Program of China (Grant No. 2022YFC330160207) and the Strategic Priority Research Program of the Chinese Academy of Sciences (Grant No. XDA19080101).

Data Availability Statement: (1) Sentinel-1A were derived from the following resources available in the public domain: [https://search.asf.alaska.edu/#/]. (2) Landsat-5, Landsat-7 , Landsat-8 were derived from the following resources available in the public domain: [https://earthexplorer.usgs.gov/]. (3) GF-1,GF-2 were derived from the following resources available in the public domain: [https://www.gscloud.cn/#page3]. (4) The one-arc-second SRTM DEM data were derived from the following resources available in the public domain: [https://earthexplorer.usgs.gov/]. (5) Precise Obit Data (POD) provided by the European Space Agency (ESA) [https://scihub.copernicus.eu/gnss/].

Acknowledgments: The Sentinel-1A data used in this study were freely provided by Copernicus and ESA, and the one-arc-second SRTM DEM data were freely downloaded from the website (https://earthexplorer.usgs.gov/) . We thank Fang Zhuo of the Wuhan University for his kind helps in revising our manuscript.

Conflicts of Interest: The authors declare no conflict of interest.

References

1. Zhao, Q.; Pepe, A.; Gao, W.; Lu, Z.; Bonano, M.; He, M.; Wang, J.; Tang, X. A DInSAR Investigation of the Ground settlement Time Evolution of Ocean-Reclaimed Lands in Shanghai. *IEEE Sel. Top. Appl. Earth Obs. Remote Sens.* **2015**, *8*, 1763–1781. [CrossRef]
2. Pepe, A.; Bonano, M.; Zhao, Q.; Yang, T.; Wang, H. The use of C-/X-band time-gapped SAR data and geotechnical models for the study of Shanghai's ocean-reclaimed lands through the SBAS-DInSAR technique. *Remote Sens.* **2016**, *8*, 911. [CrossRef]
3. Wali, M.K. *Practices and Problems of Land Reclamation in Western North America*; University of North Dakota Press: Grand Forks, ND, USA, 1975.
4. Douglas, I.; Lawson, N. Airport construction: Materials use and geomorphic change. *J. Air Transp. Manag.* **2003**, *9*, 177–185. [CrossRef]
5. De Mulder, E.; Van Bruchem, A.; Claessen, F.; Hannink, G.; Hulsbergen, J.; Satijn, H. Environmental impact assessment on land reclamation projects in the Netherlands: A case history. *Eng. Geol.* **1994**, *37*, 15–23. [CrossRef]
6. Breber, P.; Povilanskas, R.; Armaitiene, A. Recent evolution of fishery and land reclamation in curonian and lesina lagoons. *Hydrobiologia* **2008**, *611*, 105–114. [CrossRef]

7. Kooir, H. Land subsidence due to compaction in the coastal area of The Netherlands: The role of lateral fluid flow and constraints from well-log data. *Glob. Planet. Change* **2000**, *27*, 207–222.
8. Li, D.; Hou, X.; Song, Y.; Zhang, Y.; Wang, C. Ground Subsidence Analysis in Tianjin (China) Based on Sentinel-1A Data Using MT-InSAR Methods. *Appl. Sci.* **2020**, *10*, 5514. [CrossRef]
9. Gao, L. *Engineering Problems and Countermeasures of Land Reclamation in Tianjin Nangang Industrial Zone*; Tianjin University: Tianjin, China, 2015.
10. Jiang, L.; Lin, H. Integrated analysis of SAR interferometric and geological data for investigating long-term reclamation settlement of Chek Lap Kok Airport, Hong Kong. *Eng Geol.* **2010**, *110*, 77–92. [CrossRef]
11. Liu, X.; Zhao, C.; Zhang, Q.; Yang, C.; Zhang, J. Characterizing and monitoring ground settlement of marine reclamation land of Xiamen New Airport, China with Sentinel-1 SAR datasets. *Remote Sens.* **2019**, *11*, 585. [CrossRef]
12. Yu, Q.; Wang, Q.; Yan, X.; Yang, T.; Song, S.; Yao, M.; Zhou, K.; Huang, X. Ground deformation of the Chongming East Shoal Reclamation Area in Shanghai based on SBAS-InSAR and laboratory tests. *Remote Sens.* **2020**, *12*, 1016. [CrossRef]
13. Yang, M.; Yang, T.; Zhang, L.; Lin, J.; Qin, X.; Liao, M. Spatio-temporal characterization of a reclamation settlement in the Shanghai coastal area with time series analyses of X-, C-, and L-band SAR datasets. *Remote Sens.* **2018**, *10*, 329. [CrossRef]
14. Zhou, L.; Shi, X.; Ren, C.; Huang, Y.; Zhu, Z. Monitoring of Land Subsidence in Shenzhen Reclamation Area Based on Sentinel-1A Interferometric Synthetic Aperture Radar. *Sci. Technol. Eng.* **2021**, *21*, 8765–8769.
15. Chen, G.; Zhang, Y.; Zeng, R.; Yang, Z.; Chen, X.; Zhao, F.; Meng, X. Detection of land subsidence associated with land creation and rapid urbanization in the Chinese Loess Plateau using time series InSAR: A case study of Lanzhou New District. *Remote Sens.* **2018**, *10*, 270. [CrossRef]
16. Zhang, Y.; Liu, Y.; Jin, M.; Jing, Y.; Liu, Y.; Liu, Y.; Chen, Y. Monitoring land subsidence in Wuhan city (China) using the SBAS-InSAR method with radarsat-2 imagery data. *Remote Sens.* **2019**, *19*, 743. [CrossRef] [PubMed]
17. Jiang, Y.; Liao, M.; Wang, H.; Zhang, L.; Balz, T. Monitoring land subsidence in Wuhan city (China) using the SBAS-InSAR method with radarsat-2 imagery data. *Sensors* **2016**, *8*, 1021.
18. Cai, F.; Su, X.; Liu, J.; Li, B.; Lei, G. Coastal erosion in China under the condition of global climate change and measures for its prevention. *Prog. Nat. Sci.* **2009**, *19*, 415–426. [CrossRef]
19. Ma, J.; Zhou, Z.; Guo, Q.; Zhu, S.; Dai, Y.; Shen, Q. Spatial characterization of seawater intrusion in a coastal Aquifer of Northeast Liaodong Bay, China. *Sustainability* **2019**, *11*, 7013. [CrossRef]
20. Dongmeia, H.; Currellc, M. Delineating multiple salinization processes in a coastal plain aquifer, northern China:Hydrochemical and isotopic evidence. *Hydrol. Earth Syst Sci.* **2018**, *22*, 3473–3491.
21. Zhu, L.; Jiang, C.; Wang, Y.; Peng, Y.; Zhang, P. A risk assessment of water salinization during the initial impounding period of a proposed reservoir in Tianjin, China. *Sustainability* **2013**, *15*, 1743–1751. [CrossRef]
22. Bai, L.; Jiang, L.; Wang, H.; Sun, Q. Spatiotemporal Characterization of Land Subsidence and Uplift (2009–2010) over Wuhan in Central China Revealed by TerraSAR-X InSAR Analysis. *Remote Sens.* **2016**, *8*, 350. [CrossRef]
23. Liu, P.; Li, Q.; Li, Z.; Hoey, T.; Liu, G.; Wang, C.; Hu, Z.; Zhou, Z.; Singleton, A. Anatomy of Subsidence in Tianjin from Time Series InSAR. *Remote Sens.* **2016**, *8*, 45–49. [CrossRef]
24. Chen, Y. *Study on a Long Sequence of Groundwater Level Dynamic in Tianjin*; China University of Geosciences (Beijing): Beijing, China, 2015.
25. Wang, K.; Wang, W.; Li, Q.; Yu, M.; Li, P. Characteristics of changes of groundwater buried depth and influencing factors in Tianjin plain area over past 21 years. *Water Resour. Prot.* **2014**, *30*, 45–49.
26. Guo, L.; Gong, H.; Li, X.; Zhu, L.; Lv, W.; Lyu, M. Analysis of land subsidence changes on the Beijing Plain from 2004 to 2015. *Proc. Int. Assoc. Hydrol. Sci.* **2020**, *382*, 291–296. [CrossRef]
27. Ha, D.; Zheng, G.; Loaiciga, H.A.; Guo, W.; Zhou, H.; Chai, J. Long-term groundwater level changes and land subsidence in Tianjin, China. *Acta Geotech.* **2021**, *16*, 1303–1314. [CrossRef]
28. Tang, W.; Zhan, W.; Jin, B.; Motagh, M.; Xu, Y. Spatial Variability of Relative Sea-Level Rise in Tianjin, China: Insight from InSAR, GPS, and Tide-Gauge Observations. *Remote Sens.* **2021**, *14*, 2621–2633. [CrossRef]
29. Du, Q.; Li, G.; Chen, D.; Zhou, Y.; Qi, S.; Wu, G.; Chai, M.; Tang, L.; Jia, H.; Peng, W. SBAS-InSAR-Based Analysis of Surface Deformation in the Eastern Tianshan Mountains, China. *Front. Earth Sci.* **2021**, *9*, 729454. [CrossRef]
30. Li, B.; Wang, Z.; An, J.; Zhou, C.; Ma, Y. Time-Series Analysis of Subsidence in Nanning, China, Based on Sentinel-1A Data by the SBAS InSAR Method. *J. Photogramm. Remote. Sens. Geoinf. Sci.* **2020**, *88*, 291–304. [CrossRef]
31. Tao, Q.; Wang, F.; Guo, Z.; Hu, L.; Yang, C.; Liu, T. Accuracy verification and evaluation of small baseline subset (SBAS) interferometric synthetic aperture radar (InSAR) for monitoring mining subsidence. *Int. J. Remote Sens.* **2021**, *54*, 641–662. [CrossRef]
32. Zhu, C.; Zhang, Y.; Zhang, J.; Zhang, L.; Long, S.; Wu, H. Recent subsidence in Tianjin, China: Observations from multi-looking TerraSAR-X InSAR from 2009 to 2013. *Int. J. Remote Sens.* **2019**, *36*, 5869–5886. [CrossRef]
33. Liu, L.; Yuan, C. Analysis of ground subsidence in Tianjin Beijiang, Nanjiang and Dongjiang Port. *J. Waterw. Harb.* **2019**, *40*, 338–343.
34. Hu, B.; Zhou, J.; Wang, J.; Chen, Z.; Wang, D.; Xu, S. Risk assessment of land subsidence at Tianjin coastal area in China. *Environ. Earth Sci.* **2009**, *59*, 269–276. [CrossRef]

35. Liu, S.P.; Shi, B.; Gu, K.; Zhang, C.C.; Yang, J.L.; Zhang, S.; Yang, P. Land subsidence monitoring in sinking coastal areas using distributed fiber optic sensing: A case study. *Nat. Hazards* **2020**, *103*, 3043–3061. [CrossRef]
36. Yang, A.W.; Liu, Q.; Li, Z.L. Experimental Study on the Effect of Inherent Anisotropy on Strength and Deformation of Soft Soil. *J. Wuhan Univ. Technol.* **2012**, *34*, 87–91.
37. Li, X.Y.; Cheng, L.; Sha, H.L. Remote sensing analysis of tidal flat utilization characteristic of Tianjin Binhai New Area. *Mar. Sci. Bull.* **2021**, *40*, 379–386.
38. Zhu, G.; Xu, X. Annual Processes of Land Reclamation from the Sea along the Northwest Coast of Bohai Bay during 1974 to 2010. *Sci. Geogr. Sin.* **2012**, *32*, 1006–1012.
39. Xu, B.; Feng, G.; Li, Z.; Wang, Q.; Wang, C.; Xie, R. Coastal subsidence monitoring associated with land reclamation using the point target based SBAS-InSAR method: A case study of Shenzhen, China. *Remote Sens.* **2016**, *8*, 1006–1652. [CrossRef]
40. Chen, Y.; Yu, S.; Tao, Q.; Liu, G.; Wang, L.; Wang, F. Accuracy verification and correction of D-InSAR and SBAS-InSAR in monitoring mining surface subsidenc. *Remote Sens.* **2021**, *13*, 4365. [CrossRef]
41. Yao, J.; Yao, X.; Liu, X. Landslide detection and mapping based on SBAS-InSAR and PS-InSAR: A case study in Gongjue County, Tibet, China. *Remote Sens.* **2022**, *14*, 4728. [CrossRef]
42. Chen, D.; Chen, H.; Zhang, W.; Cao, C.; Zhu, K.; Yuan, X.; Du, Y. Characteristics of the residual surface deformation of multiple abandoned mined-out areas based on a field investigation and SBAS-InSAR: A case study in Jilin, China. *Remote Sens.* **2020**, *12*, 3752. [CrossRef]
43. Festa, D.; Bonano, M.; Casagli, N.; Confuorto, P.; De Luca, C.; Del Soldato, M.; Casu, F. Nation-wide mapping and classification of ground deformation phenomena through the spatial clustering of P-SBAS InSAR measurements: Italy case study. *ISPRS J. Photogramm. Remote. Sens.* **2022**, *189*, 1–22. [CrossRef]
44. Wu, Q.; Jia, C.; Chen, S.; Li, H. SBAS-InSAR based deformation detection of urban land, created from mega-scale mountain excavating and valley filling in the Loess Plateau: The case study of Yan'an City. *Remote Sens.* **2019**, *11*, 1673. [CrossRef]
45. Costantini, M. A novel phase unwrapping method based on network programming. *IEEE Trans. Geosci. Remote.* **1998**, *36*, 813–821. [CrossRef]
46. Zhang, Y.; Meng, X.; Jordan, C.; Novellino, A.; Dijkstra, T.; Chen, G. Investigating slow-moving landslides in the Zhouqu region of China using InSAR time series. *Remote Sens.* **2018**, *15*, 1299–1315. [CrossRef]
47. Zhao, X.; Wang, L.; Ma, Y.; Wang, J.; Yang, X.; Yang, X.; Xing, J.; Jin, B. Monitoring and analysis of surface deformation in land reclamation area based on SBAS-InSAR technology: Take Tianjin port for example. *Mar. Sci. Bull.* **2022**, *2*, 17–30.
48. Hu, R.L.; Wang, S.J.; Lee, C.F.; Li, M.L. Characteristics and trends of land subsidence in Tanggu, Tianjin, China. *Bull. Eng. Geol. Environ.* **2002**, *61*, 213–225.
49. Zhang, T.; Shen, W. B.; Wu, W.; Zhang, B.; Pan, Y. Recent surface deformation in the Tianjin area revealed by Sentinel-1A data. *Remote Sens.* **2019**, *11*, 130. [CrossRef]
50. Li, J.; Tang, H.; Rao, W.L.; Zhang, L.; Sun, W.K. Influence of South-to-North Water Transfer Project on the changes of terrestrial water storage in North China Plain. *J. Univ. Chin. Acad. Sci.* **2020**, *37*, 775–783.
51. Yu, W.; Gong, H.; Chen, B.; Zhou, C.; Zhang, Q. Combined GRACE and MT-InSAR to Assess the Relationship between Groundwater Storage Change and Land Subsidence in the Beijing-Tianjin-Hebei Region. *Remote Sens.* **2021**, *13*, 3773. [CrossRef]
52. Samieie-Esfahany, S.; Hanssen, R.F.; van Thienen-Visser, K.; Muntendam-Bos, A. On the effect of horizontal deformation on InSAR subsidence estimates. *ESA-SP* **2010**, *39*, 677.

Disclaimer/Publisher's Note: The statements, opinions and data contained in all publications are solely those of the individual author(s) and contributor(s) and not of MDPI and/or the editor(s). MDPI and/or the editor(s) disclaim responsibility for any injury to people or property resulting from any ideas, methods, instructions or products referred to in the content.